NONINVASIVE MONITORING OF CCl_4 INDUCED ACUTE AND CHRONIC LIVER DAMAGE IN RAT BY SINGLE QUANTUM AND TRIPLE QUANTUM FILTERED ^{23}Na MAGNETIC RESONANCE IMAGING

YONG GAO

Submitted to the faculty of the University Graduate School
in partial fulfillment of the requirements
for the degree
Master of Science
in the Department of Cellular & Integrative Physiology
Indiana University

October 2008

Accepted by the Faculty of Indiana University, in partial fulfillment of the requirements for the degree of Master of Science.

Master's Thesis Committee

Navin Bansal, Ph.D., Chair

Andriy M. Babsky, Ph.D.

Stephen A. Kempson, Ph.D.

David P. Basile, Ph.D.

ACKNOWLEDGEMENTS

First and foremost, I would like to express profound gratitude to my esteemed advisor, Dr. Navin Bansal, for his invaluable support, encouragement, supervision and suggestions throughout my graduate study. His moral support and continuous guidance enabled me to complete my research work successfully.

I am also grateful to the members of my graduate committee for their assistance in my study. Special thanks go out to Dr. Andriy Babsky for his valuable guidance and help in my experiments. Thanks are also due to Dr. Stephen Kempson and Dr. David Basile for their suggestions on my thesis writing.

I would like to thank Judy James for her useful advice and collaboration in my research. She has impressed me with her willingness to share with me her knowledge and experience in MRI study.

Finally, and most importantly, I am forever indebted to my parents and my wife, Dr. Fang Wang, for their understanding, encouragement and endless love when it was most required.

ABSTRACT

Yong Gao

NONINVASIVE MONITORING OF CCl_4 INDUCED ACUTE AND CHRONIC LIVER DAMAGE IN RAT BY SINGLE QUANTUM AND TRIPLE QUANTUM FILTERED ^{23}Na MAGNETIC RESONANCE IMAGING

In present study, single quantum (SQ) and triple quantum filtered (TQF) ^{23}Na magnetic resonance imaging (MRI) was used to monitor the severity and progression of CCl_4 induced acute and chronic liver damage in rat model. SQ ^{23}Na MRI was proposed to measure the ^{23}Na signal intensity (SI) of total tissue sodium ions, and TQF ^{23}Na MRI was proposed to measure the SI of intracellular sodium ions. In addition, shift reagent aided ^{23}Na and ^{31}P magnetic resonance spectroscopy (MRS) was used to measure *in vivo* intracellular sodium concentration ($[Na^+_i]$), total tissue sodium concentration ($[Na^+_t]$) and relative extracellular space (rECS) of liver in the same model.

In acute high dose CCl_4 intoxication, 24 hours after single dose of CCl_4 in 5ml per kg body weight of mixture of CCl_4 and oil in 1:1 ratio, SQ ^{23}Na SI increased by 83% and TQF ^{23}Na SI increased by 174% compared to the baseline level. According to SR-aided ^{23}Na and ^{31}P MRS, $[Na^+_i]$ increased by 188% and $[Na^+_t]$ increased by 43%. In addition, there was significant decrease in cellular energetic level, represented by ATP/P_i ratio.

Histology examination showed pronounced inflammatory response in centrilobular regions, with neutrophiles infiltration, fatty accumulation and swollen hepatocytes.

In chronic 8-week experiment, chronic damage was induced by biweekly administration of CCl_4 in a dosage of 0.5 ml per kg body weight. From week 1 to week 6, SQ ^{23}Na SI remained relatively constant, and then increased by 15% from week 6 to week 8. TQF ^{23}Na SI progressively increased from week 1 to week 8, totally by 56%. Both SQ and TQF ^{23}Na SI showed significant difference between treated group and control at every week. SR-aided ^{23}Na and ^{31}P MRS experiment showed that, at the end of 8-week CCl_4 intoxication, both $[Na^+_t]$ and rECS were higher than control, by 49% and 47% respectively; however, there was no significant difference for $[Na^+_i]$ between two groups. Histology examination showed excessive deposition of extracellular matrix.

In conclusion, SQ and TQF ^{23}Na MRI appears valuable in the functional assessment of liver in noninvasive approach, and could be a promising diagnostic modality for liver diseases in clinical area.

Navin Bansal, Ph.D.

Committee Chair

TABLE OF CONTENTS

LIST OF TABLES

LIST OF FIGURES

LIST OF ABBREVIATIONS

ALT	alanine aminotransferase
AMP	adenosine monophosphate
ADP	adenosine diphosphate
AST	aspartate aminotransferase
ATP	adenosine triphosphate
BW	body weight
CCl_4	carbon tetrachloride
Cr	creatine
CT	computerized tomography
DQ	double quantum
ECS	extracellular space
FID	free induction decay
FOV	field of view
Gro	readout gradient
Gpe	phase encoding gradient
HSCs	hepatic stellate cells
MQF	multiple quantum filtered
MR	magnetic resonance
MRI	magnetic resonance imaging
MRS	magnetic resonance spectroscopy
Na^+_e	extracellular sodium

Na^{+}_{i}	intracellular sodium
Na^{+}_{t}	total tissue sodium
PCr	phosphocreatine
P_i	inorganic phosphate
ppm	parts per million
rDW	relative dry to wet weight ratio
rECS	relative extracellular space
RF	radio frequency
rICS	relative intracellular space
SNR	signal to noise ratio
SQ	single quantum
SR	shift reagent
T_1	longitudinal relaxation time constant
T_2	transverse relaxation time constant
TE	echo time
$TmDOTP^{5-}$	thulium-1,4,7,10-tetraazacyclododecane 1,4,7,10-tetrakis(methylene phosphonate)
TQ	triple quantum
TQF	triple quantum filtered
TR	repetition time

INTRODUCTION

Liver is the central organ for metabolism and detoxification in human body, which leaves it vulnerable to various risk factors, like metabolic disorders, alcohol consumption, viral infection or toxin exposure. Currently, liver disease is ranked the 8th most deadly disease worldwide [1]. Because most of the liver diseases are chronic and progressive, it is desirable to accurately monitor the progression of chronic liver disease so as to choose and assess the appropriate therapeutic strategies, like chemotherapy, radiation therapy, or liver transplantation [2-4].

Currently, liver biopsy is still the gold standard to detect and grade the liver disease. However, this method has a few limitations, such as possible injury to patients as an invasive procedure, false negative results and being not convenient for frequent operations on patients. Therefore, it is necessary to find appropriate supplementary techniques to noninvasively detect and monitor the progression of liver diseases.

Single quantum (SQ) and triple quantum filtered (TQF) ^{23}Na magnetic resonance imaging (MRI) has been proposed as a noninvasive method that allows one to differentiate and measure the intracellular and extracellular sodium MR signal and does not require infusion of an exogenous chemical shift reagent (SR) [5-10]. This technique depends on the different relaxation characteristics of free/unbound extracellular Na^+ and protein-bound intracellular Na^+. SQ ^{23}Na MRI is used to acquire the signal from the total tissue sodium, which mainly comprise the unbound extracellular Na^+ for the high concentration of Na^+ in extracellular space, and TQF ^{23}Na MRI is used to acquire the signal from protein-bound intracellular Na^+ [11]. Because sodium MR signal is closely related to the sodium concentrations, thus, this technique could be used to monitor the sodium concentration changes in biological systems. On the other hand, changes in sodium concentration are always the reflection of the changes in the dynamic cellular homeostasis, and disruption of this homeostasis can be seen in diseased states, like ischemia or tumors [12, 13], therefore, this technique holds the promise to monitor the severity and progression of the injury.

This technique has been evaluated in several *in vivo* studies to monitor the ^{23}Na SI changes during tumor growth and response to chemotherapies, proved to be sensitive in probing the relationship between sodium signal and tumor growth or necrosis [2, 14-16]. The present study was designed to evaluate the utility of SQ and TQF ^{23}Na MRI in assessing the rat liver injury in CCl_4-induced hepatotoxic model, and at the same time, SR-aided ^{23}Na and ^{31}P MRS was performed to measure the real time intracellular and extracellular sodium concentrations in this model. Data from SR-aided experiments were used to validate and also delineate the mechanisms behind the ^{23}Na signal changes measured by ^{23}Na MRI.

CHAPTER 1

OBJECTIVES

Aim 1: *In vivo* SQ and TQF ^{23}Na MR imaging of rat liver in acute and chronic carbon tetrachloride (CCl_4) induced hepatotoxic model. Acute and chronic liver injuries were induced by oral administration of CCl_4 in rats. SQ ^{23}Na MRI would be used to collect the ^{23}Na signal of the total tissue Na^+, and TQF ^{23}Na MRI was expected to filter out the signal from free or unbound Na^+ and collect only the signal from the protein-bound Na^+.

Hypothesis: In CCl_4-induced liver injury, it was expected that cell membrane was damaged and the permeability to ions was increased, resulting to an elevated $[Na^+_i]$. In chronic experiment with CCl_4 administration, liver fibrosis was expected with abundant formation of extracellular fibrils, which could be monitored and interpreted as an increased signal from protein-bound extracellular Na^+ by TQF ^{23}Na MRI. The total ^{23}Na signal by SQ ^{23}MRI could also be increased for the increased extracellular space after excessive deposition of extracellular matrix.

Aim 2: *In vivo* quantitation of $[Na^+_i]$ and $[Na^+_e]$ and monitoring of cellular energetic status in the rat liver in acute and chronic CCl_4 induced hepatotoxic model. The hyperfine SR, $TmDOTP^{5-}$, would be used to differentiate the intracellular and extracellular Na^+ signals, and also measure the extracellular space with the help of ^{23}Na MRS and ^{31}P MRS. The cellular energetic status during liver injury would be monitored by ^{31}P MRS. The concentration of ATP and intracellular pH would be calculated from the ^{31}P MRS spectra.

Hypothesis: In liver injury by CCl_4, the cellular membrane integrity could be damaged and the membrane permeability to outside Na^+ will be increased, which will elevate the $[Na^+_i]$, and it has been found the intracellular energetics would also be compromised and the intracellular pH would be decreased.

CHAPTER 2

BACKGROUND AND SIGNIFICANCE

2.1. CCl_4 induced toxicological model in rats

CCl_4 has been widely used as a solvent and cleaner in industry and household, and currently its usage is restricted to research area because of its distinct toxicity to liver [17]. CCl_4-induced liver injury in animals has been proved to be highly useful as an experimental model to study the mechanism underlying the hepatotoxic effects, like hepatitis and fibrosis [17].

The CCl_4 induced hepatotoxicity is related to dose and duration. At high dose and short term, acute toxicity ensues with hepatocellular necrosis and accumulation of inflammatory cells in centrilobular regions and also significant fat droplet deposition in hepatocytes [18]. At low dose and prolonged expose, a mixed response of liver injury and regeneration comes afterward, often leading to fibrosis and cirrhosis in the late stage. Currently, the most clearly illustrated mechanism underlying the CCl_4 induced liver injury has been related to the production of reactive radicals and lipid peroxidation [17, 19, 20].

In hepatocytes, CCl_4 is transformed into CCl_3* by cytochrome P450 in endoplasmic reticulum. CCl_3* is a free radical and can react with various biological substances, like proteins, nucleotides and lipids. Furthermore, in the presence of oxygen, the CCl_3* radical is converted to the trichloromethyl peroxy (CCl_3OO*), which is a more reactive radical and can cause more widespread damage than CCl_3*. CCl_3OO* is more likely to abstract a hydrogen from unsaturated poly fatty acids, e.g. the lipids in membrane, resulting to lipid peroxidation with the formation of reactive aldehydes, carbonyls and alkanes. These radicals will carry on the CCl_4 hepatotoxic effects by binding to a variety of biological molecules and disrupt their normal functions [17].

CCl_4 has been widely used in inducing liver fibrosis and cirrhosis with long term administration in numerous studies [19, 21-24]. The underlying mechanism behind fibrosis was proposed as a complex of inflammatory and regenerative responses [17, 23, 24]. It was found that the activation of hepatic stellate cells (HSCs), also known as lipocytes or Ito cells, plays a key role during the long process of liver fibrosis [22, 23, 25, 26]. HSCs could be activated by a variety of growth factors and cytokines, especially the transforming growth factor beta 1 (TGFβ1), which are derived from other liver cells, like damaged hepatocytes, and activated HSCs, or infiltrating inflammatory cells in liver parenchyma. Activation of HSCs causes the proliferation of HSCs and transformation of HSCs to fibrogenic myofibroblasts, which can overproduce numerous extracellular matrix proteins and result to liver fibrosis.

2.2 Sodium as a biomarker for cellular activities

In normal biological condition, there is a stable sodium concentration gradient across the cell membrane, with an intracellular concentration of ~15 mM and an extracellular concentration of ~140 mM. This trans-membrane gradient is maintained by the Na^+/K^+ pump in the cell membrane, which utilizes ATP to pump sodium ions out of the cell and potassium ions into the cell. This Na^+ gradient plays a very important role in cellular activities, like regulating cell volume, playing a role in action potential, and is also used to drive the transport of various nutrients and ions into or out of the cells. For instance, intracellular pH is regulated by Na^+/H^+ exchanger to pump excess H^+ out of the cells, and Na^+-glucose co-transporter drives the glucose into the cells.

The sodium gradient could be disrupted in many pathological conditions, where the abnormal cellular metabolism, such as shortage of ATP availability and excessive intracellular acid production, could increase the intracellular $[Na^+]$. Therefore, sodium concentration could be an indicator of cellular integrity and metabolic homeostasis [27]. It has been found that cell division and the acidic extracellular microenvironment in malignancies are associated with an increase of intracellular Na^+ concentration [28-30].

2.3 ^{23}Na magnetic resonance techniques

Because of its high tissue concentration, 100% natural abundance, and short T_1, ^{23}Na is the second most sensitive magnetic resonance nucleus in biological tissues, with only ^{1}H being more sensitive. However, one difficulty with ^{23}Na MR study is that the MR signal from intra and extracellular sodiums are isochronous, therefore, simple spectroscopy or imaging techniques can not differentiate the two sources of ^{23}Na signals and monitor either changes. To circumvent this difficulty, two approaches of paramagnetic SRs and MQF technique have been developed to discriminate between Na^+_i and Na^+_e signals.

2.4 SR aided ^{23}Na MR spectroscopy

SR is a negatively charged complex containing a lanthanide metal ion (Dy^{3+}, Tm^{3+} or Tb^{3+}) which alters the resonance frequency of the cations, like Na^+, to which it binds. Because it is charged molecule, SR usually can not freely pass through the cell membrane and can only bind to Na^+_e. When SR binds with Na^+_e, it can greatly alter the relaxation characteristics of the Na^+_e so that the resonance signal from Na^+_e is altered, while at the same time, the resonance signal from Na^+_i is not affected, which make it possible to discriminate between the signals from intra or extra-cellular sodium ions.

A new kind of SRs, $TmDOTP^{5-}$ (Figure 1), has been shown to bring improvement over the dysprosium based SR and produce clear resolved resonance peaks from intra and extra Na^+ with minimal interference with the animal physiology [16, 31]. This SR has a net negative charge at physiological pH value but has a more favourable geometry for Na^+ binding, which produces a better shift.

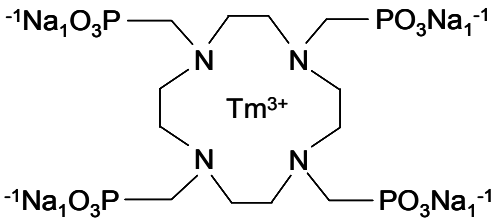

Figure 1. Structure of $TmDOTP^{5-}$.

2.5 MQF ^{23}Na MR spectroscopy

Another method is the MQF technique which utilizes the unique ^{23}Na relaxation properties to distinguish between Na^+_i and Na^+_e. ^{23}Na has a spin quantum number I=3/2, and four possible spin orientations and three possible single quantum transitions: one inner transition of -1/2 to +1/2, and two outer transitions of -3/2 to -1/2 and +1/2 to +3/2, shown in Figure 2. It was found that when the correlation time of Na^+, τ_C, is longer than the larmor period, ω_L-1, the two outer transitions will relax more quickly than the inner transition [32]. These two distinct relaxation rates in certain condition for inner and outer transitions make it possible to bring out the double quantum transitions of -3/2 to +1/2 and 1/2 to 3/2, and the triple quantum transition of -3/2 to +3/2. Because there is a high concentration of macromolecules in intracellular space, like protein molecules, the Na_i^+ is more likely to bind with macromolecules than the free unbound Na_e^+. Binding with macromolecules could increase the τ_C of Na^+_i, which results to two transition rates for intracellular sodium and brings a strong MQF signals from within the cell, but virtually none from outside of the cell.

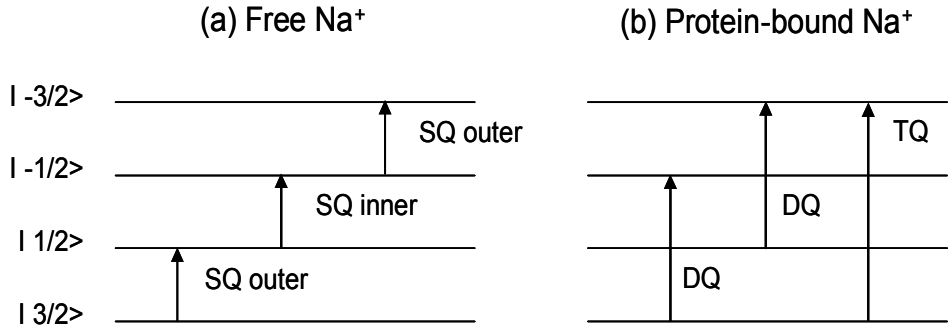

Figure 2. Energy level diagram for ^{23}Na (I = 3/2) showing the four possible energy states. In the case of free Na^+ ions, only SQ transitions are possible (a). When the Na^+ ions are transiently bound to protein, the SQ outer transitions relax faster than the inner transition, and DQ and TQ transitions become possible (b).

2.6. SQ and MQF ^{23}Na MR imaging

In MRI, the three main sources of contrast in constructing an image are differences in spin density, longitudinal relaxation time constant (T_1) and transverse relaxation time constant (T_2). Compared to ^{1}H MRI, which is usually T_1 or T_2 weighted, the main problem with ^{23}Na MRI is its relatively short T_1 or T_2 relaxation time in tissue, although ^{23}Na MRI still could be acquired to be T_2 weighted. Therefore, the spin density of Na^+ concentration is more likely to be utilized to construct ^{23}Na image. Because changes in [Na^+] is closely related to cellular activities, so ^{23}Na MRI can yield specific functional imaging.

The potential of TQF technique to mainly collect signal from intracellular Na^+ has stimulated the research on TQF imaging in phantom and animal studies [5, 8, 9, 33]. Various TQF imaging sequences had been tested to produce the best signal to noise ratio (SNR) in phantom studies and was applied in rat kidney studies to measure the cellular injury after ischemia [6]. In addition, two techniques were devised to further improve the SNR in TQF imaging. The first was called weighted signal submission, which works by collecting maximum signal averages when the phase-encoding gradient is minimum and reducing the number of signal averages as the gradient amplitude increases. This technique can improve the SNR by 50%. The second technique is called coherent summation of multiple echoes. With this method, a multi-echo data set is collected using repeated reversal of the read-out gradient. The alternate echoes in the multi-echo data set are reversed and then all the echoes are added together, which was proved to result in ~ 60% increase in SNR.

2.7 ^{31}P MR Spectroscopy in liver

With a 100% natural abundance and being the third most sensitivity relative to ^{1}H, ^{31}P is the most widely used nucleus to study *in vivo* metabolic process and energetic status, for phosphorus metabolites play a key role in metabolic reactions involving energy production and transfer. These metabolites are also used to regulate and fine tune many

metabolic pathways. Because liver is an organ with a robust role in metabolism, ^{31}P MR could be an optimal tool to noninvasively monitor and study the metabolism and energetics in liver.

The typical ^{31}P spectrum of rat liver is shown in Figure 3. The resonance for phosphomonoesters (PME) contains contributions from a number of small molecular weight phosphorylated intermediates, like phosphocholine (PC), phosphoethanolamine (PE), adenosine monophosphate (AMP), and glycolytic intermediates. Elevated level of PME signal usually implies biosynthesis of phospholipid and membrane remodeling, which could happen in some disease states, like liver cirrhosis and tumors [34]. The resonance of PDE mainly contains contributions from glycerophosphorylacholine (GPC) and glycerophosphorylethanolamine (GPE), which are produced by sequential hydrolysis of phospholipids by phospholipases A1 and A2, and represents membrane degradation. Because PME and PDE usually develop in opposite direction, the ratio of PME and PDE is often calculated as robust marker for membrane metabolism. High levels of PME/PDE have been reported in hepatic tumors and in regenerating lives following hepatic resection [34].

Inorganic phosphate (P_i) is produced by a number of phosphoesterases, and plays a major role in ATP synthesis, either in oxidative pathway or in glycolytic pathway. The P_i resonance could be used to measure intracellular pH, because the chemical shift of P_i, relative to the α–ATP signal, is sensitive to pH changes. pH is calculated using the Henderson-Hasselbach equation, as followed:

$$pH = 6.76 + \log\left[\frac{\delta_{P_i-\alpha ATP} - 10.85}{13.25 - \delta_{P_i-\alpha ATP}}\right],$$

Where δ is the chemical shift in ppm for P_i resonance signal.

α-, β- and γ-ATPs are energy rich compounds. α–phosphate is the primary phosphate of nucleoside tri- and di-phosphates. γ–phosphate is the terminal phosphate of nucleotide

tri- and di-phosphates. β–phosphate is the middle phosphate of nucleoside triphosphates only. ^{31}P MRS can detect these compounds at a concentration above 1 mM. In normal condition, those energetic compounds are maintained in a relatively constant level through homeostatic process, however, in pathological states, like cancers, the levels of those compounds could be changed [27, 35].

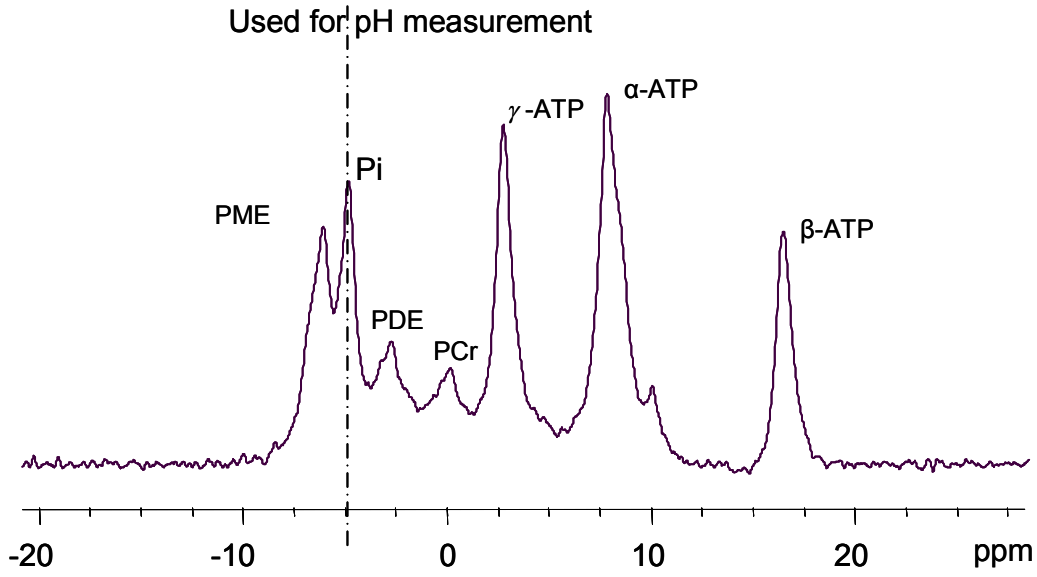

Figure 3. *In vivo* ^{31}P MR spectrum of rat liver showing resonances (from left to right) from PME, PDE, Pi, and three phosphate groups of ATP molecule; γ-ATP, α-ATP and β–ATP.

CHAPTER 3

METHODS

3.1 Acute and chronic CCl_4 liver injury animal models

Acute CCl_4-induced hepatotoxic experiments were performed on two groups of male Wistar rats (200 - 300 g, n = 8 in each group), shown in Table 1; the rats in CCl_4 group were given a single oral dose of 5 ml/kg body weight (BW) of a CCl_4 and corn oil mixture (ratio 1:1), and the rats in the control group received a single dose of 5 ml/kg BW of corn oil. SQ and TQF ^{23}Na MRI experiments were performed on the CCl_4 group before and 24 hr after the treatment. SR-aided ^{23}Na and ^{31}P MRS experiments were performed on the control and CCl_4 groups 24 hr after the treatment.

For chronic CCl_4-induced hepatotoxic experiments two groups of Wistar rats (70 - 80 g, n= 7 in each group) were studied, shown in Table 1. The rats in CCl_4 group initially underwent Phenobarbital (0.35 ml per liter of drinking water) treatment for two weeks. Subsequently, 1 ml/kg BW of a CCl_4 and corn oil mixture (ratio 1:1) were given orally twice per week for eight weeks. The rats in control group underwent the same treatment as the CCl_4 group except that only 1 ml/kg BW of oil was given orally. Phenobarbital water treatment went throughout the total 10 weeks. The animal weights were recorded before each oral treatment. SQ and TQF ^{23}Na MRI experiments were performed on both the groups before and on weeks 2, 4, 6 and 8 after initiating the CCl_4 treatment. SR-aided ^{23}Na and ^{31}P MRS experiments were performed on all the rats on week 8 after the last ^{23}Na MRI experiment.

Table 1. Animal grouping in acute and chronic CCl_4-induced hepatotoxic experiments on rats.

	Dose	**CCl_4**	**Oil**	**n**
Acute – 24 hours				
Control	Single	-	5.0 ml/kg	8
Treated	Single	2.5 ml/kg	2.5 ml/kg	8
Chronic – 8 weeks				
Control	Twice Weekly	-	1 ml/kg	7
Treated	Twice Weekly	0.5 ml/kg	0.5 ml/kg	7

Note: Acute intoxication was induced by CCl_4 in a dose of 2.5ml/kg BW and duration of 24 hours. Chronic intoxication was induced by CCl_4 in a bi-weekly dose of 0.5ml/kg BW and duration of 8 weeks.

3.2 SQ and MQF ^{23}Na MRI

All *in vivo* MR experiments were performed with a Varian 9.4 Tesla 31-cm diameter actively shielded horizontal bore MR system. The system is equipped with a 12 cm diameter gradient insert capable of generating 38 gauss/cm gradient strength in all three directions.

A 50 mm diameter and 30 mm high loop-gap resonator tuned to 106 MHz was used for SQ and TQF ^{23}Na MRI experiments. A 10 mm NMR tube filled with 50 mM NaCl solution was placed beside the internal wall of the coil to serve as a ^{23}Na MRI signal intensity standard. The rats were anesthetized with 1-2% isofluorane in medical air at a flow rate of 2 ml/min for SQ and TQF ^{23}Na MRI experiments. Warm air was blown through the magnet bore to maintain the animal core body temperature at 34-35 °C, which was monitored with a fiber optic probe (FISO Technologies Inc., Quebec, Canada). The magnet was shimmed to less than 100 Hz line-width at half-height of the ^{23}Na signal.

SQ ^{23}Na MR images of the abdomen were obtained using a three-dimensional (3D) gradient-echo imaging sequence and the following imaging parameters: 100-130 μs 90° excitation RF pulse, 50 ms repetition-time (TR), 4.5 ms echo-time (TE), and 64 × 64 × 16 data points over a 60 × 60 × 60 mm field of view (FOV). The weighted signal summation (WSS) technique was employed in the two phase-encoding directions to improve SNR. A maximum of 64 and an average of 9.67 signal transients were collected for the phase-encoding steps. Total data collection time for the 3D ^{23}Na image was 10 minutes.

TQF ^{23}Na MR images of the tumor were obtained using the pulse sequence shown in Figure 4. This sequence is essentially a concatenation of a three-pulse TQ filter with a 3D gradient-echo imaging sequence. This imaging sequence produces the optimum SNR and fewest image artifacts compared to the TQF imaging sequences in which the phase-encoding gradients are applied during the preparation time or evolution time. The other imaging parameters were: 100-130 μs 90° RF pulses, 100 ms TR, 4.5 m TE, and 64 × 32 × 8 data points over a 60 × 60 × 60 mm FOV. An optimum preparation time of 4.5 ms, which gives maximum SNR, was used. The evolution time was kept as short as possible (10 μs) to reduce signal loss due to TQ T_2 but allow RF phase switching. The WSS technique with a maximum of 384 and an average of 109.22 signal averages was employed to increase SNR. The number of acquisitions was increased in steps of 6 to complete the basic phase-cycle necessary for selecting a TQ coherence. Total data collection time for TQF ^{23}Na MRI was 55 minutes.

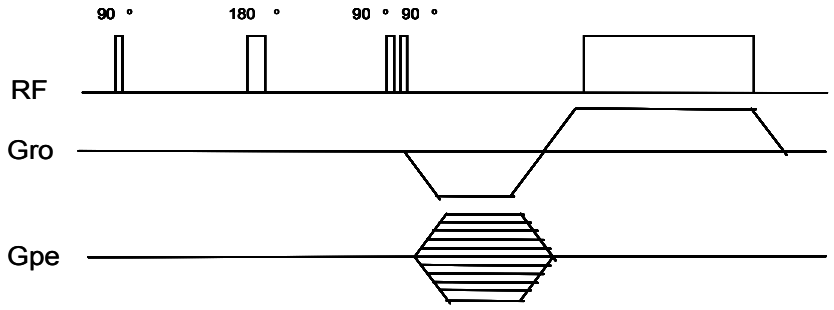

Figure 4. Gradient echo imaging sequence for TQF ^{23}Na MRI. The readout dephasing gradient (Gro) and phase-encoding gradient (Gpe) are applied after all the RF pulses, and a gradient echo is formed along the readout direction.

SQ and TQF ^{23}Na MRI time-domain data were zero-filled to 128 × 128 × 16 and Fourier-transformed. ROI were drawn outlining the liver region, and the signal intensities of SQ and TQF ^{23}Na MRI were calculated as the ratios to that of 50 mM NaCl solution reference.

3.3 SR-Aided ^{23}Na and ^{31}P MRS

A 2 cm diameter surface coil dual-tuned to 106 and 163 MHz was used for SR-aided ^{23}Na and ^{31}P MRS experiments. A small glass bulb (~300 μL) containing 150 mM NaCl and 20 mM $TmDOTP^{5-}$ at pH 5.0 was placed in a holder in the center of the surface coil and used as an external concentration standard. This solution provided external reference signals for both the ^{23}Na and ^{31}P spectra. The ^{23}Na signal shifted by ~10 ppm was used as the reference for tissue ^{23}Na signal. The ^{31}P signal from the four equivalent phosphonate groups of $TmDOTP^{5-}$, shifted to -315 ppm (by lowering the pH), was used as a reference for the tissue $TmDOTP^{5-}$ signal at about -330 ppm. The nominal 90° excitation pulse-width at the coil center was 55 μs for ^{23}Na and 50 μs for ^{31}P during the calibration and the *in vivo* experiments.

The ^{23}Na and ^{31}P signals from the reference bulb were calibrated before the *in vivo* experiments using ~60 ml volume plastic bags filled with NaCl and $TmDOTP^{5-}$solutions. Seven bags filled with 10-70 mM NaCl were used for calibration of the ^{23}Na signal, and 13 bags filled with 0.2 to 3.0 mM $TmDOTP^{5-}$ were used to calibrate the ^{31}P signal. Eight of the $TmDOTP^{5-}$ bags were filled with 60 mM NaCl, and the other eight were filled with 150 mM NaCl to examine the effects of coil loading the calibration. The bags were positioned under the dual-tuned surface coil, and ^{23}Na or ^{31}P spectra were collected and processed by using the same parameters as in the *in vivo* experiments. The ratio of the peak areas from either Na^+ or $TmDOTP^{5-}$ in the bags, relative to the corresponding reference in the bulb vs. the known concentration of Na^+ or $TmDOTP^{5-}$ in the bag is shown in Figure 5. A least squares linear regression of the data yielded calibration slopes of 0.0288 ± 0.0010, respectively, for ^{23}Na (r^2 = 0.99) and slope and intercept of 0.984 ± 0.021 and -0.194 ± 0.028, respectively, for ^{31}P (r^2 = 0.98).

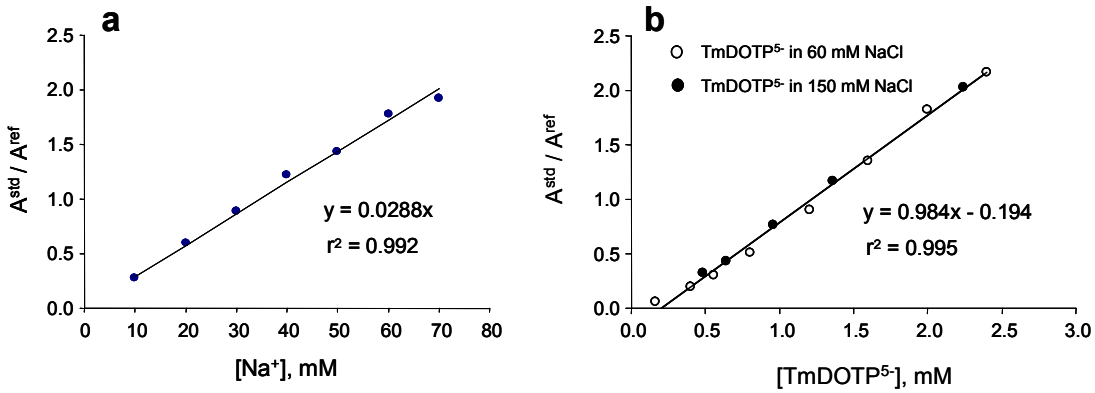

Figure 5. Calibration curves for ^{23}Na and ^{31}P spectroscopy; (a) integrated areas of Na^+ in sealed bags at serial concentrations vs. 150 mM Na^+ from a reference tube. (b) integrated areas of $TmDOTP^{5-}$ in sealed bags at serial concentrations vs. 20 mM $TmDOTP^{5-}$ from the reference tube.

The rats were surgically prepared for SR infusion and for placement of the dual-tuned surface coil on the liver. After assuring adequate depth of anesthesia with isofluorane, a jugular vein was cannulated through a midline neck incision for infusion of the SR. A nephrorectomy was performed to prevent the clearance of $TmDOTP^{5+}$ through the kidneys. A laparotomy was performed, and the liver was exposed through a subcostal incision. The liver was covered with a single layer of Saran wrap and the surface coil was placed over the liver. Animals were positioned supine in a specially constructed cradle and poisoned inside the magnet. The animal core body temperature was maintained at 34-35 °C by blowing warm air through the magnet bore.

The surface coil was initially tuned to the ^{23}Na frequency and the magnet was shimmed to 60-70 Hz line-width at half-height of the ^{23}Na signal. The coil was then tuned to ^{31}P frequency, and then, a set of baseline ^{31}P tissue metabolite and $TmDOTP^{5-}$ spectra was collected before SR infusion. The coil was re-tuned to ^{23}Na frequency and ^{23}Na spectra were continuously collected during SR infusion. An 80 mM $Na_4HTmDOTP$ (Macrocyclics, Dallas, TX) stock solution, prepared in deionized water, was initially infused at a rate of 0.03 ml/min for 6 min. The rate was increased to 0.06 ml/min for 6 min, and then to 0.1 ml/min for another 6 min. After that the rate was maintained at 1.3

ml/min for 20-30 min. After a chemical shift separation of 3-4 ppm was achieved between the intra- and extracellular Na^+ resonances, the infusion rate was reduced to 0.03-0.04 ml/min for 10-15 minutes to attain a stable shift of extracellular Na^+ resonance.

In vivo ^{23}Na and ^{31}P from the rat liver were collected using a pulse-acquire sequence. ^{23}Na spectra were collected using a 100 ms pre-delay, 2,000 data points (real + imaginary) over a spectral width of 10,000 Hz, and 128 signal averages over ~40 s. ^{31}P spectra of the liver phosphorus metabolites and $TmDOTP^{5-}$ were collected separately because the phosphonate group of $TmDOTP^{5-}$ resonate -300 ppm away from the tissue metabolite signals. ^{31}P metabolite spectra were collected using a pre-delay of 1 s, 4,000 data points over a spectral width of 8,000 Hz, and 256 signal averages over ~290 s. ^{31}P spectra of $TmDOTP^{5-}$ were collected using a pre-delay of 10 ms, 2,000 data points over 20,000 Hz spectral width, and 1024 signal transients over 62 s. All time domain data were Fourier transformed after baseline correction, zero-filling once, and multiplication by a single exponential corresponding to a 10-Hz line broadening for ^{23}Na, a 25-Hz line broadening for ^{31}P metabolites, and a 100-Hz line broadening for $TmDOTP^{5-}$. The peak areas were determined by integration between user defined intervals. Peak area ratios between the tissue and the corresponding reference bulb signals were then calculated, and tissue concentrations were determined from the ^{23}Na and ^{31}P reference calibration curves as described below. The results from three consecutive steady-state spectra were averaged.

The concentration of $TmDOTP^{5-}$ in tissue, $[TmDOTP^{5-}]_{tissue}$, was determined from the peak areas of the ^{31}P $TmDOTP^{5-}$ resonance from the tissue (A_{tissue}^{Tm}), the reference bulb (A_{ref}^{Tm}) and the reference calibration constants by using the following equation,

$$[TmDOTP^{5-}]_{tissue} = \frac{1}{1.44}\left(\frac{A_{tissue}^{Tm}}{A_{ref}^{Tm}} + 0.22\right)$$

The concentration of $TmDOTP^{5-}$ in extracellular space, ($[TmDOTP^{5-}]_{ext}$) was determined from the chemical shift separation (in ppm) between Na_e^+ and Na_i^+ resonances in the in vivo ^{23}Na spectra by using the following equantion,

$$[TmDOTP^{5-}]_{ext} = \frac{1}{1.06}(\delta_{Na_e} - \delta_{Na_i} + 0.4)$$

The relative extracellular space (rECS) was calculated by using the relation,

$$rECS = \frac{[TmDOTP^{5-}]_{tissue}}{[TmDOTP^{5-}]_{ext}}$$

The relative intracellular space was calculated from the rECS and rDW by using the relation,

$$rICS = 1 - rECS - rDW$$

The sodium concentration in cellular water ($[Na^+]_i$) was calculated from the peak areas of the Na_i^+ (A_{tissue}^{Tm}), reference resonances in ^{23}Na spectra, the reference calibration constants, and the rICS by using the following equation,

$$[Na^+]_i = \frac{1}{1.44 \times rICS}\left(\frac{A_{tissue}^{Na}}{A_{ref}^{Na}} + 0.22\right)$$

After the ATP peak collection, the coil was tuned back to ^{23}Na and power arrayed for finding the best 90º pulse for ^{23}Na spectroscopy.

3.4 Histological examination

After the SR-aided MRS experiments, rats were sacrificed. Livers were excised, and one lobe of liver tissue was fixed in zinc-formalin solution (Anatech, Battle Creek,, MI) and embedded in paraffin. Liver tissue slices sectioned ~ 5 μm thicknesses were stained with hematoxylin and eosin (H&E). Digital microscopic images of the liver sections were taken in 100× and 400× magnification. Another lobe of liver was weighted and dried to measure the ratio of wet tissue to dried tissue.

CHAPTER 4

RESULTS

4.1 Effect of CCl_4 on animal body weight

In acute intoxication experiment, 24 hours after the high dose CCl_4 treatment, the average animal weight decreased by 7% (from 241±23 to 224±22 g, P<0.0005). In chronic intoxication experiment, before starting the oil or CCl_4 treatment, the average body weight of control or experimental rats was ~170g around 6-week old, then, through the eight-week study, the CCl_4-treated rats showed an retarded growth and the body weight was less than that of control rats of the same age (333±7 and 371±2 g, respectively, at week 8, P<0.001), shown in Figure 6.

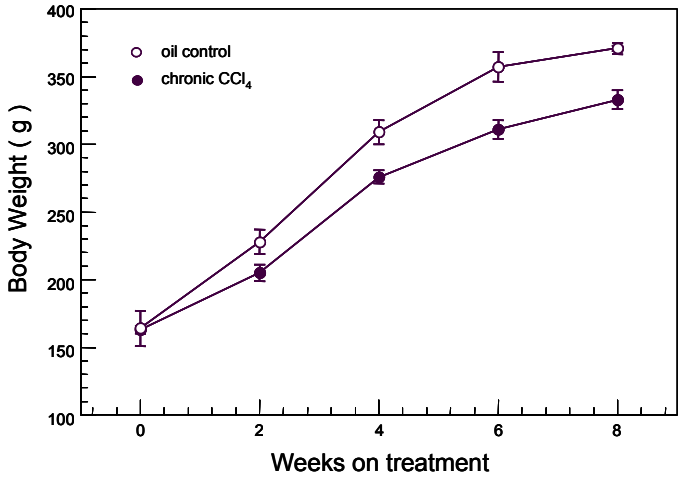

Figure 6. Effect of CCl_4 treatment on rat weight. The average weight of CCl_4 treated rats was less than that of control rats of the same age. (P< 0.05, * - vs. control of the same age)

4.2 *In vivo* SQ and TQF ^{23}Na MR imaging experiments

Figure 7 shows the representative transaxial slices from 3D SQ and TQF ^{23}Na MR images of the rat liver before and 24 hours after the high dose CCl_4 treatment. The increase of ^{23}Na signal intensity both in SQ and TQF MRI can be clearly seen as changes in color from green to red. Reference tube with 50 mM NaCl appeared in the SQ ^{23}Na

MRI but not in the TQF ^{23}Na MR images, which proved the effective filtering of SQ ^{23}Na signal in TQF ^{23}Na MRI. Region of interest (ROI) was drawn in white circle to cover the liver without including the kidney and vasculature. The increase in ^{23}Na signal intensity of ROIs in SQ and TQF MRI display a remarkable increase. The SQ ^{23}Na SI of rat liver, relative to the reference, increased from 0.60±0.03 to 1.10±0.02 (P<0.05) and TQF ^{23}Na SI increased from 0.35±0.11 to 0.96±0.12 (P<0.05), before and 24 hours after CCl_4 treatment, shown in Figure 8.

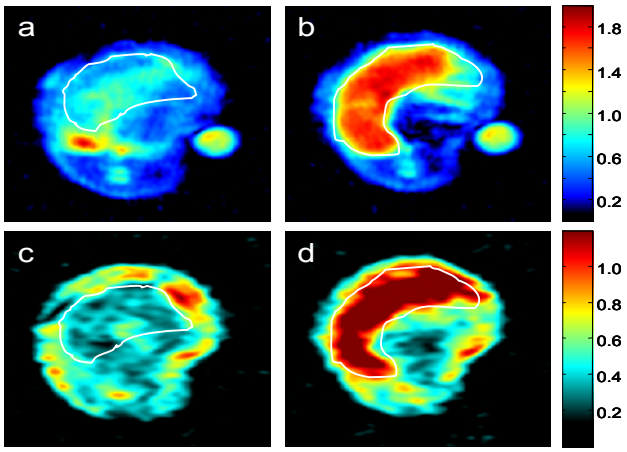

Figure 7. Representative slices from a 3D SQ (a, b) and TQF (c, d) ^{23}Na MRI of rat liver before (a, c) and after (b, d) acute CCl_4 intoxication (5ml/kg bw of mixture of CCl_4 and oil in 1:1 ratio). The region of liver was marked by white line.

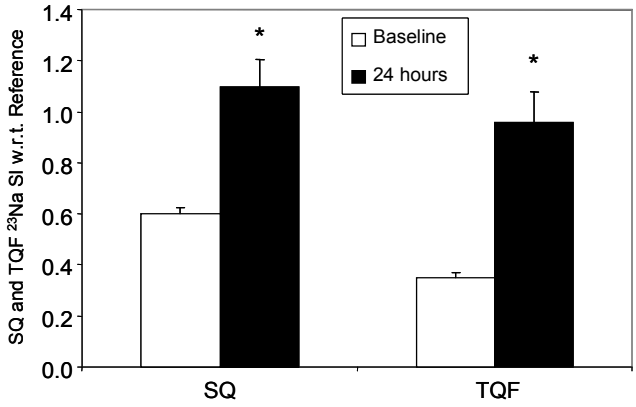

Figure 8. Effects of high-dose acute CCl_4 intoxication on SQ and TQF ^{23}Na SI of rat liver. The ^{23}Na SI in SQ and TQF MRI increased by 80% and 90% respectively, 24 hours after the treatment, compared with baseline data.(from 0.6±0.03 to 1.1±0.02; 0.35±0.11 to 0.96±0.12, *P<0.05)

In chronic CCl_4 intoxication experiment, the representative transaxial slices from 3D SQ and TQF ^{23}Na MR images of the rat livers through week 0 to week 8 were shown in Figure 9. ROIs of rat liver were circled in white line. The graph of ^{23}Na SI through 8-week experiment, relative to reference, is shown in figure 10. For SQ MRI, in CCl_4 treatment group, the average ^{23}Na SI were 0.69±0.03 before CCl_4 treatment. Along with the CCl_4 treatment, the SI remained relatively constant from week 1 to week 6 but afterwards increased significantly from 0.70±0.01 to 0.87±0.03 (P<0.05) from week 7 to week 8, while in the control group, the SI changed in a downshift trend, decreasing continuously from 0.77±0.05 before oil treatment to 0.51±0.02 at week 8 (P<0.05). For TQF MRI in CCl_4 group (Figure 11), the average SI was 0.32±0.03 before CCl_4 treatment, then steadily increased by 64% over the 8-week period, from 0.40±0.02 at week 2, 0.42±0.02 at week 4, 0.46±0.02 at week 6 to 0.52±0.02 at week 8. The statistically significant increase happened from week 1 to week 2 and from week 6 to week 8, while the SI increases from week 2 to week 4 and from week 4 to week 6 were not significant statistically. In control rats, the overall change of SI through 8 weeks showed a downshift trend, from 0.37±0.08 at week 0 to 0.23±0.02 at week 8 (P<0.05).

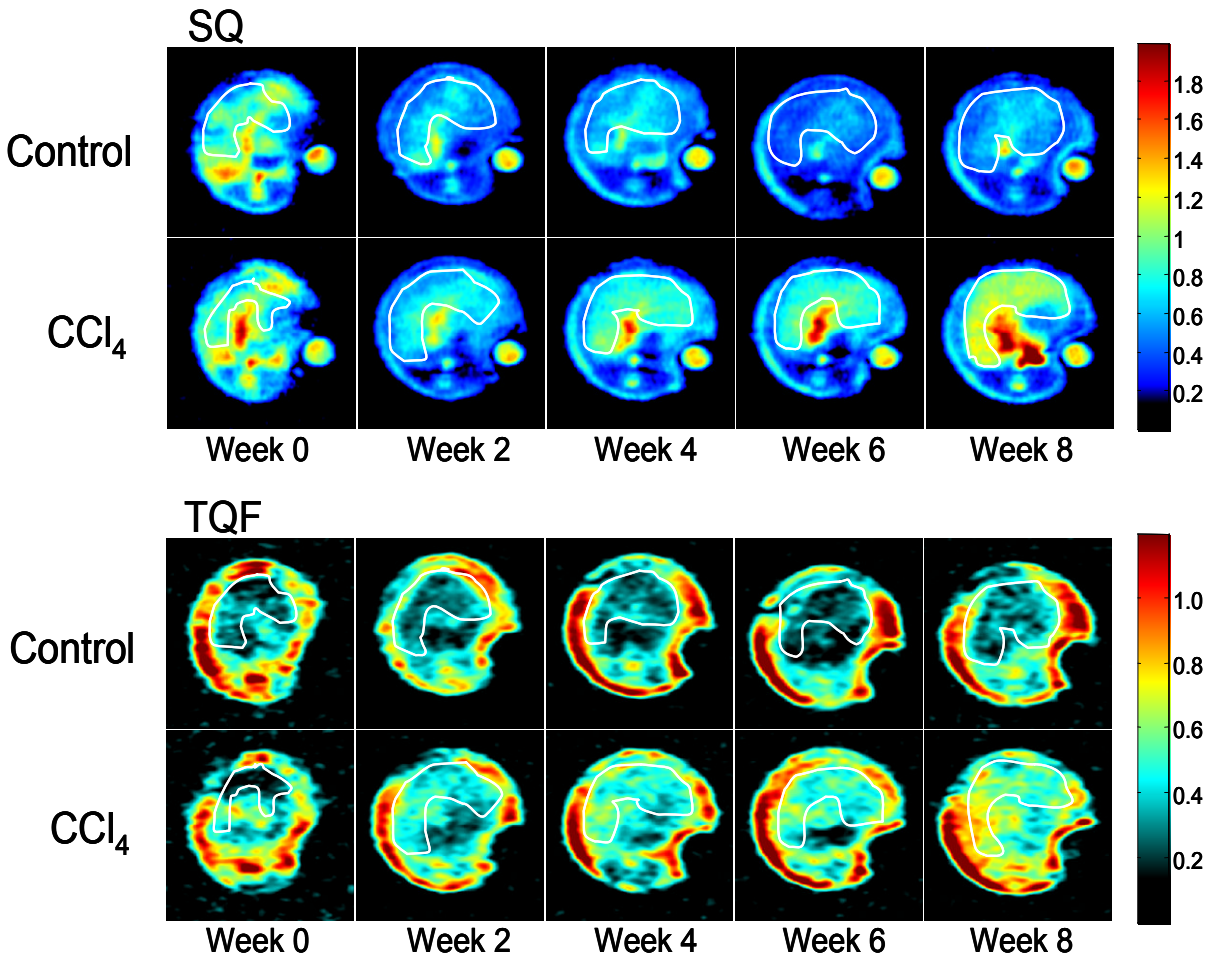

Figure 9. Representative slices from a 3D SQ and TQF ^{23}Na MRI of rat liver during 8-week study. The liver regions were marked by white line. SQ and TQF ^{23}Na SI of rat liver in CCl_4 treated rats increased continuously shown in color change.

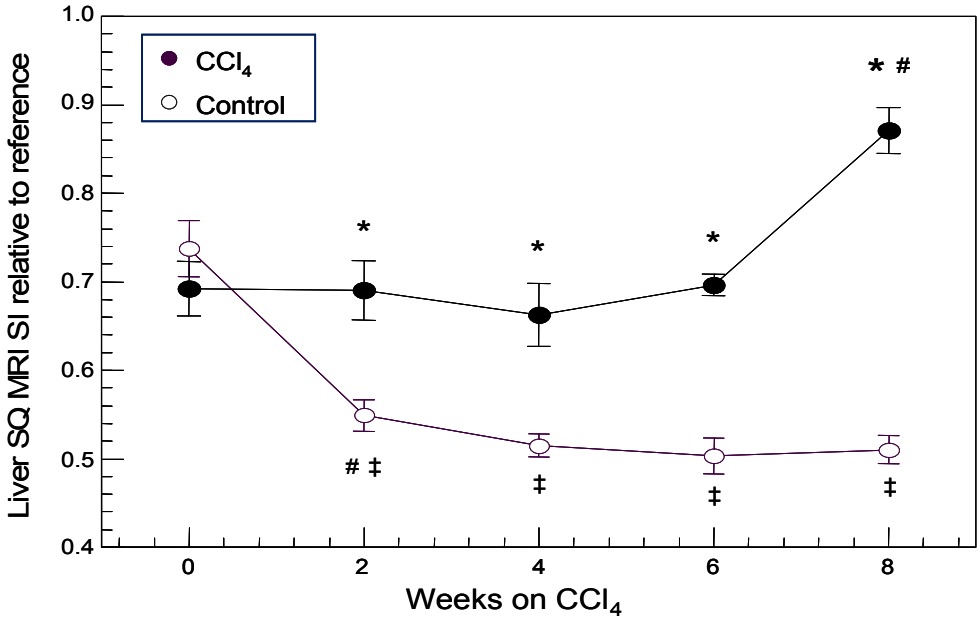

Figure 10. Effect of chronic low dose CCl_4 intoxication on SQ ^{23}Na SI. The SI of control and treated rats was ~0.7 with no significant difference, then following the treatment, SI of CCl_4-treated rat was much higher than control at every time point, and also had a sharp increase by 25% from week 6 to week 8. ($P< 0.05$, * - vs. control, $^{\#}$ - vs. previous time point, ‡ - vs. week 0)

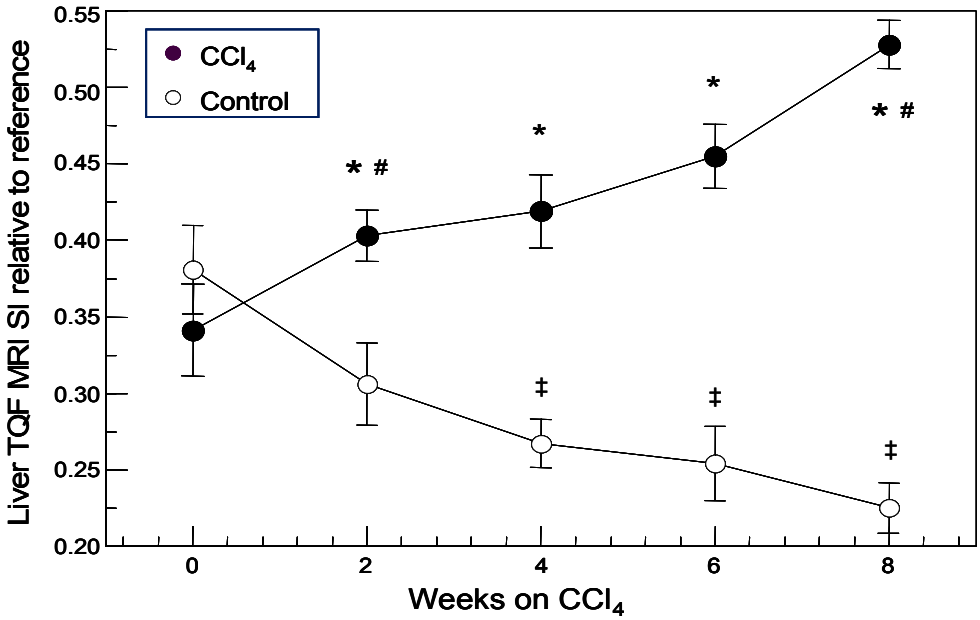

Figure 11. Effect of chronic low dose CCl_4 intoxication on TQF ^{23}Na SI. The SI of control and treated rats were ~0.35 with no significant difference, then following the

treatment, SI of CCl_4-treated kept increasing and was much higher than those of control at every time point. At week 8, SI of CCl_4 treated rats was 135% higher than control. ($P< 0.05$, * - vs. control, $^{\#}$ - vs. previous time point, ‡ - vs. week 0)

4.2 *In vivo* SR-aid ^{23}Na and ^{31}P spectroscopy

Representative *in vivo* ^{23}Na and ^{31}P spectra of control rat liver before and after infusion of $TmDOTP^{5-}$ are shown in Figure 12. Before infusion of SR, the intra and extracellular Na^+ resonance peaks were isochronous (set to 0 ppm). After infusion of SR, the extracellular Na^+ resonance peak shifted about 5 ppm downfield, while the intracellular Na^+ resonance remained at 0 ppm. The ^{23}Na resonance peak at 12 ppm originated from Na^+ in the reference bulb. In ^{31}P spectra, the two peaks at ~315 ppm were from the $TmDOTP^{5-}$ in the same reference bulb. The peak at ~325 ppm was from the SR in the rat liver after infusion of $TmDOTP^{5-}$ and is closely related to the size of the rECS. In ^{31}P-metabolites spectra, the three phosphate groups in ATP molecule gave three separated peaks, and the areas under curve of the ATP peaks were no significant difference ($P<$ 0.05) before and after infusion of $TmDOTP^{5-}$. The PCr peak of phosphocreatine was from the muscle of neighboring tissues, like diaphragm, abdominal wall or intestine, and was kept small by a careful placement of the surface coil to obtain minimal touching with those tissues. The peak of organic phosphate (P_i) and the peak of phosphomonoesters (PME) were also acquired from the liver tissue.

Figure 13 shows the typical ^{23}Na and ^{31}P spectra of rat livers in acute and chronic CCl_4 experiments. Compared to the ^{23}Na spectra in control rats, the intracellular Na^+ peak in acute CCl_4 treated rats and the extracellular Na^+ peak in chronic CCl_4 treated rats became significantly enlarged. Also, the ^{31}P-SR peak in chronic CCl_4 group is shown to be obviously higher than that in control group, which implies enlarged rECS. There is not remarkable difference in APT specs between control rats and CCl_4 treated rats.

The quantitative data acquired by ^{23}Na and ^{31}P MRS are summarized in Table 2 and 3. In acute CCl_4 experiment, the values of rECS, rICS, and rDW do not show much difference between control rats and CCl_4-treated rats, however, for $[Na^+_i]$, there is significant increase from 17 ± 2 to 49 ± 7 (P<0.01), and also for $[Na^+_t]$, from 32±2 to 46±4 (P<0.01). The ATP/P_i ratio, which stands for cellular energetics, had a significant decrease between 1.24±0.08 and 0.94±0.10 (P<0.05) in control and CCl_4 treated rats, respectively.

In chronic CCl_4 experiment, the rDW of liver shows a significant decrease between CCl_4 treated rats and control rats (0.22±0.01 and 0.28±0.11, $P<0.05$). The rECS was significantly higher in CCl_4-intoxicated rats (0.28±0.03) than in controls (0.19±0.03; $P<0.05$), and $[Na^+_t]$ was significantly higher in the CCl_4-treated rats (52±7) than in the controls (35±4, $P<0.05$). There is no significant change in $[Na^+_i]$ between two groups. For cellular energetics and pH, there is also no significant change between two groups.

In summary, compared to control rats, acute CCl_4 treatment caused a significant increased in $[Na^+_i]$ and $[Na^+_t]$, and chronic CCl_4 treatment caused a significant increase in rECS and $[Na^+_t]$.

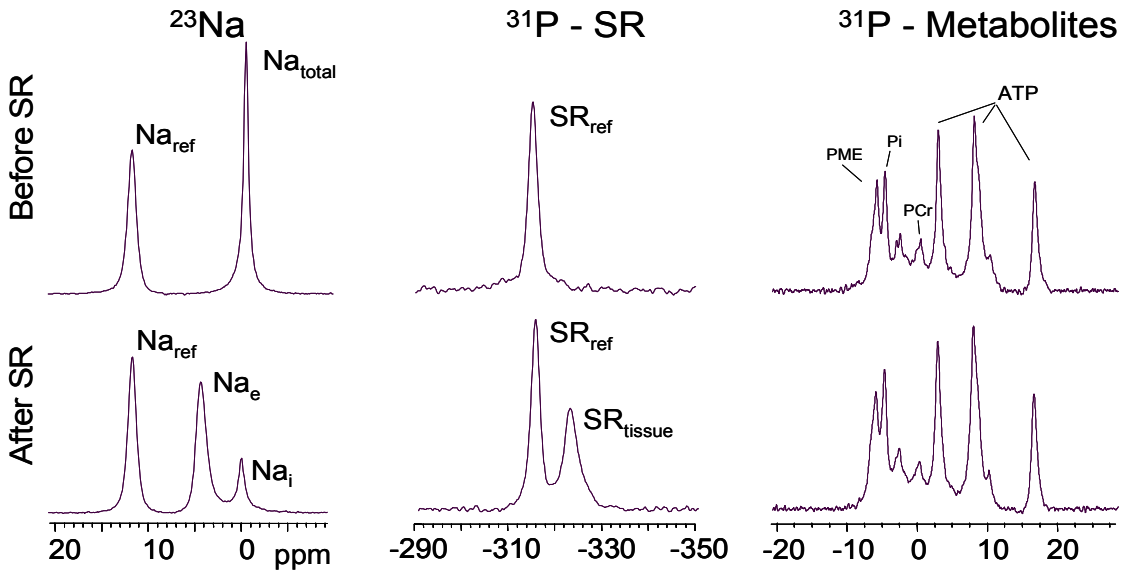

Figure 12. Representative *in vivo* ^{23}Na and ^{31}P spectra of control rat before and after infusion of SR. Na^{+}_{e} resonance shifted away from Na_i about 4 ppm and $TmDOTP^{5-}$ resonance from liver tissue appeared about 12 ppm away from reference after infusion of SR. ^{31}P metabolites resonances are not different before and after infusion of SR.

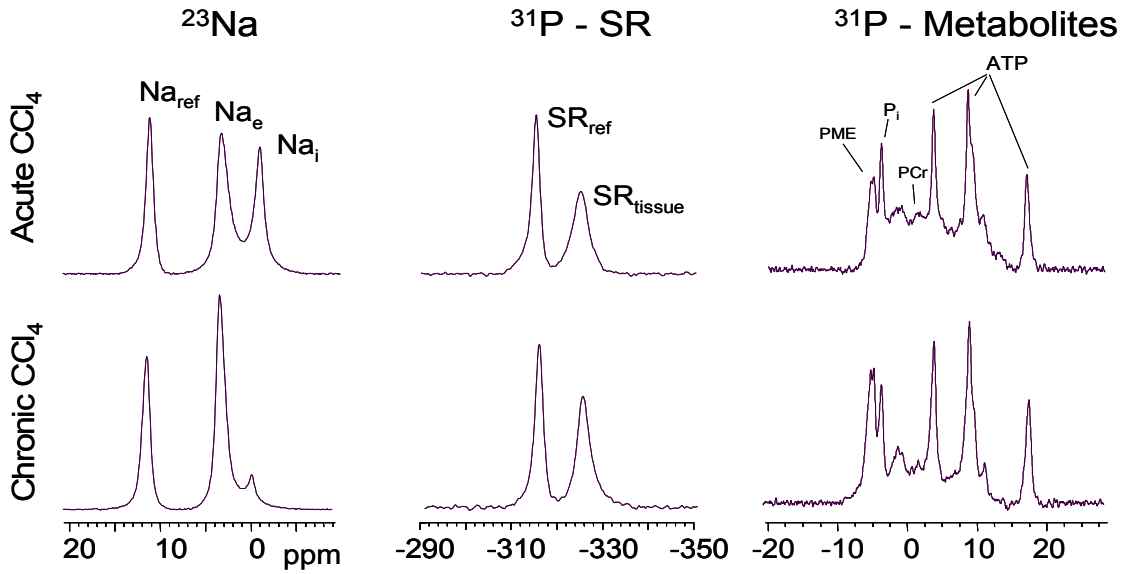

Figure 13. Representative ^{23}Na and ^{31}P spectra of rat liver after infusion of SR in acute CCl_4 treated rats and chronic CCl_4 treated rat at week 8. Na_i resonance grew much larger in acute CCl_4 intoxication while Na_e resonance grew much larger in chronic CCl4 intoxication, compared to reference. SR resonance from liver tissue also grew much larger compared to SR reference in chronic CCl4 intoxication.

Table 2. Comparison of parameters of liver tissue by ^{23}Na and ^{31}P spectroscopy between control and CCl_4 treated rats in high dose acute experiment. (* - $P<0.05$)

	Control	CCl_4	P-values
rDW	0.27 ± 0.01	0.27 ± 0.01	0.72
rECS	0.24 ± 0.02	0.26 ± 0.01	0.22
rICS	0.49 ± 0.02	0.47 ± 0.02	0.35
$[Na^+_t]$, mM	32 ± 2	46 ± 4 *	0.005
$[Na^+_i]$, mM	17 ± 2	49 ± 7 *	0.0005
ATP/Pi	1.24 ± 0.08	0.94 ± 0.10 *	0.012
pH	7.33 ± 0.02	7.29 ± 0.01	0.66
$[Mg^{2+}_{free}]$	563 ± 26	540 ± 37	0.63

Table 3. Comparison of parameters of liver tissue measured by ^{23}Na and ^{31}P spectroscopy between control and CCl_4-treated rats in low dose chronic experiment. (* - $P<0.05$)

	Control	CCl_4	P-values
rDW	0.28 ± 0.01	0.22 ± 0.01 *	< 0.0001
rECS	0.19 ± 0.03	0.28 ± 0.03 *	0.03
rICS	0.53 ± 0.03	0.50 ± 0.03	0.35
$[Na^+_t]$, mM	35 ± 4	52 ± 7 *	0.04
$[Na^+_i]$, mM	18 ± 2	18 ± 2	0.93
ATP/Pi	1.24 ± 0.12	1.35 ± 0.07	0.59
pH	7.36 ± 0.04	7.29 ± 0.03	0.28
$[Mg^{2+}_{free}]$	661 ± 43	572 ± 41	0.27

4.3 Liver histology

The light microscopic images of rat liver slices of control and CCl_4 treated rats by H&E staining were shown in Figure 14. In acute experiment, 24 hours after high dose CCl_4 treatment, acute inflammatory response was shown mainly in the centrilobular regions, like neutrophils infiltration, significant fatty infiltration in hepatocytes and hepatocellular necrosis with swollen cells and dissolved nucleus.

In chronic experiment, 8 weeks after low dose CCl_4 treatment, there were abundant and extensive collagen bundles in liver parenchyma and mild fatty infiltration in hepatocytes.

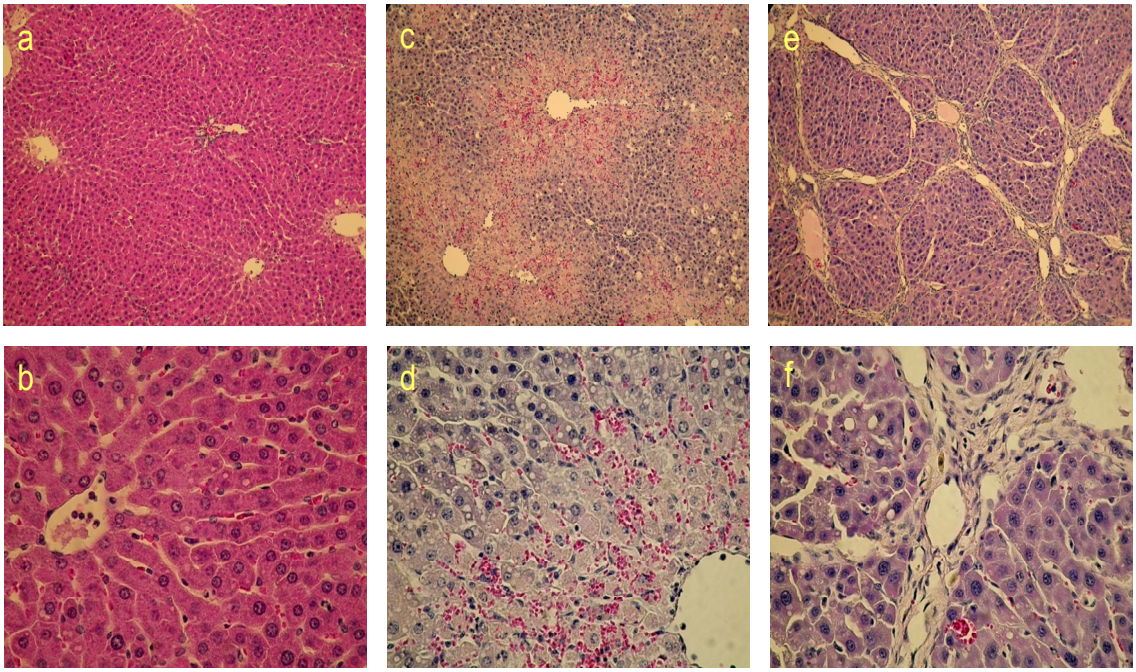

Figure 14. Histological examination of rat liver slices by H& E staining in 100× (up row) and 400× (down row) magnification. (a,b) Slices of normal control rat liver. (c,d) acute CCl_4 induced liver injury, shown with inflammatory response in centrilobular regions, like fatty deposition, neutrophils infiltration and hepatocellular necrosis. (e,f) chronic CCl_4 induced liver injury, shown with abundant collagen bundles.

CHAPTER 5

DISCUSSION

To be able to noninvasively detect and monitor the extent and progression of liver disease, especially the chronic liver disease, is a major priority in clinical area. A variety of diagnostic modalities such as laboratory liver function tests, ultrasonography, computerized tomography (CT) and MRI, have been proposed to try to accomplish this aim and yet remain under extensive evaluation [4, 11, 36-40]. Laboratory tests, including measurements of aspartate aminotransferase (AST) to alanine aminotransferase (ALT) ratio, AST to platelet ratio index (APRI), or FibroTest, a composite of five serum biochemical markers of α-2-macroglobulin, apolipoprotein A1, haptoglobin, γ-glutamyltranspeptidase, and bilirubin, are closely related to hepatocellular function. However, all of the serum based tests have their cited variation in specificity and sensitivity [38]. For example, AST/ALT test has been found to be not very specific due to the enzymatic sources outside of liver. FibroTest is only useful in diagnosing significant fibrosis and cirrhosis, and suffers from poor sensitivity for mild liver disease, such as early to intermediate fibrosis and steatosis [38]. The noninvasive imaging modalities, including ultrasonography, MRI or contrast-enhanced MRI, and CT, are more related to the gross morphologic or physical features of liver, like stiffness, shape or anatomic relationship to neighboring organs. Thus, their specialties are more targeted on assessment of well-developed liver fibrosis and have limited diagnostic utility in monitoring the whole progression of liver disease, especially in detection of liver disease at its early stage and diffuse liver disease [38, 41].

Based on the knowledge that sodium ions play an important role in normal hepatocelluar activities and the ionic homeostasis could be disrupted due to the compromised cellular integrity and energy status in disease states, the current study evaluated the performance of SQ and TQF ^{23}Na MRI technique in monitoring the severity and progression of the rat liver injury in CCl_4 induced hepatotoxic model. In addition, SR-aided ^{23}Na and ^{31}P MRS

was employed in the same model to validate and find the mechanisms behind the changes in ^{23}Na MRI SI following CCl_4 intoxication treatment.

The data presented in this study shows that, in acute high dose CCl_4 intoxication experiment, 24 hours after CCl_4 treatment, the SQ ^{23}Na SI of rat liver increased by 80% and TQF ^{23}Na SI increased by 70%, compared with the baseline data before treatment. The pronounced increase in SQ ^{23}Na SI is similar to the results from other studies [42, 43], which used ^{1}H and ^{23}Na MRI to measure the CCl_4-induced liver tissue damage. According to those studies, the SIs of liver both in ^{1}H and ^{23}Na MRI increased, and it was thought that a build-up of both water and sodium ion in hepatocytes was the reason behind the increase as a result of cytotoxic edema. In current study, the subsequent SR-aided ^{23}Na and ^{31}P MRS experiment found that $[Na^{+}_{i}]$ of liver tissue in CCl_4-treated rat increased by 174%, compared to baseline data. The histological examination showed widespread swollen hepatocytes in centrilobular regions. CCl_4 could damage the cell membrane through lipid peroxidation mechanism and increase its permeability to extracellular ions, including Na^{+}, with results of elevated $[Na^{+}_{i}]$ and hepatocellular water retention [44]. Furthermore, in SR-aided MRS, it was found that the cellular energetic status, as measured by ATP/Pi ratio, was significantly decreased 24 hours after the CCl_4 treatment, which suggested that the $[Na^{+}_{i}]$ could also be increased due to reduced activity of Na^{+}/K^{+} pump for shortage of ATP supply. In TQF ^{23}Na MRI, the considerable increase of ^{23}Na SI was the direct result of the large increase in $[Na^{+}_{i}]$. Actually, the percentages of increase, in ^{23}Na SI measured by TQF ^{23}Na MRI and $[Na^{+}_{i}]$ measured by SR-aid ^{23}Na MRS, were almost the same, to be 180% and 174% respectively.

In chronic CCl_4 intoxication experiment, the results display a different scenario compared with those in the acute experiment. SQ ^{23}Na SI of CCl_4 treated rat liver first remained relative constant up to 6 weeks from start, but it was significantly higher than that in control rats. Then, the SI increased by 15% from week 7 to week 8. In TQ ^{23}Na MRI, the value of SI went up all the way from start, especially during two periods, that is, by 18% increase from week 0 to week 2 and 16 % increase from week 6 to week 8, while the SI in control rats kept significantly much lower. In SR-aided MRS, in CCl_4 treated rats, the

measured [Na^+_t] and rECS increased by ~49% and ~48%, compared to those in control group at week 8. As a number of researches had found that, in chronic liver disease, there exists a mixed process of liver damage and recovery [19, 23, 45]. The early significant increase in SQ ^{23}Na SI, compared to control, could be due to the initial injury from week 1 to week 2, which reversed the down shifting trend of SI in control rats. Then afterwards, from week 3 to week 6, the recovery process began to develop and compensate for the disrupted hepatic functions, e.g., to maintain the homeostasis of water and salts content in liver tissue. This process might explain the relatively constant level of SQ ^{23}Na SI from week 3 to week 6. However, after week 6, the compensatory mechanism began to collapse in the face of persistent CCl_4-induce damage. Thus, accelerated retention of water and salts in liver occurred, resulting to significant increase in SQ ^{23}Na SI. This process was consistent with the findings in a variety of studies, which discovered that moderate or advanced liver fibrosis started around or after 6 weeks in long term CCl_4-induced experiment [19, 24, 39].

As for TQF MRI, ^{23}Na SI displayed an ever-increasing trend. There are two possible explanations behind this trend; one could be due to the continual increase in [Na^+_i] and the other could be due to the continual built-up of extracellular protein matrix, and the later can also increase the rECS. Taking into account of the data from ^{23}Na and ^{31}P MRS, which demonstrated that rECS was increased by ~48% at week 8 compared to control rats; therefore, the abundant deposition of extracellular matrix protein could be a main reason behind the increased TQF ^{23}Na SI. This conclusion was in accordance with the histology study and also with the finding of some studies [24, 46], that liver fibrosis began to take a full-fledged role in pathologic changes after week 6, like overproduction of collagen fibers and accumulation of extracellular matrix. This finding can explain why there was a steeper increase in TQF ^{23}Na SI from week 7 to week 8. As for the role of Na^+_i, because there was no significant difference in [Na^+_i] between control and CCl_4 treated rats at week 8, the sharp increase in TQF ^{23}Na SI might be not closely related to the changes in [Na^+_i].

Overall, SQ and TQF ^{23}Na MRI appears valuable in the functional assessment of the liver in a noninvasive approach. The present research represents the first application of both SQ and TQF ^{23}Na MRI technique in monitoring the acute and chronic liver injury in CCl_4-induced rat model. Furthermore, compared to SQ ^{23}Na MRI, the TQF ^{23}Na MRI technique might be more sensitive in monitoring the progression of chronic liver damage in that the contrast in TQF ^{23}Na SI between treated rats and control rats is much higher than that in SQ ^{23}Na SI. ^{23}Na and ^{31}P MRS study was also the first application in this model for validation of the results of ^{23}Na MRI. In conclusion, with proven sensitivity and specificity, SQ and TQF ^{23}Na MRI could be promising diagnostic modality for liver diseases in clinical area.

REFERENCES

1. Kim, W.R., et al., *Burden of liver disease in the United States: summary of a workshop.* Hepatology, 2002. **36**(1): p. 227-42.
2. Babsky, A.M., et al., *Application of 23Na MRI to monitor chemotherapeutic response in RIF-1 tumors.* Neoplasia, 2005. **7**(7): p. 658-66.
3. He, S.X., et al., *Effects of extract from Ginkgo biloba on carbon tetrachloride-induced liver injury in rats.* World J Gastroenterol, 2006. **12**(24): p. 3924-8.
4. Huwart, L., et al., *Magnetic resonance elastography for the noninvasive staging of liver fibrosis.* Gastroenterology, 2008. **135**(1): p. 32-40.
5. Griffey, R.H., B.V. Griffey, and N.A. Matwiyoff, *Triple-quantum-coherence-filtered imaging of sodium ions in vivo at 4.7 tesla.* Magn Reson Med, 1990. **13**(2): p. 305-13.
6. Bansal, N. and V. Seshan, *Three-dimensional triple quantum-filtered 23Na imaging of rabbit kidney with weighted signal averaging.* Journal of Magnetic Resonance Imaging, 1995. **5**(6): p. 761-7.
7. Boada, F.E., et al., *Non-invasive assessment of tumor proliferation using triple quantum filtered 23/Na MRI: technical challenges and solutions.* Conf Proc IEEE Eng Med Biol Soc, 2004. **7**: p. 5238-41.
8. Hancu, I., F.E. Boada, and G.X. Shen, *Three-dimensional triple-quantum-filtered (23)Na imaging of in vivo human brain.* Magn Reson Med, 1999. **42**(6): p. 1146-54.
9. Kalyanapuram, R., V. Seshan, and N. Bansal, *Three-dimensional triple-quantum-filtered 23Na imaging of the dog head in vivo.* Journal of Magnetic Resonance Imaging, 1998. **8**(5): p. 1182-9.
10. Reddy, R., E.K. Insko, and J.S. Leigh, *Triple quantum sodium imaging of articular cartilage.* Magn Reson Med, 1997. **38**(2): p. 279-84.
11. Aube, C., et al., *Diagnosis and measurement of liver fibrosis by MRI in bile duct ligated rats.* Dig Dis Sci, 2007. **52**(10): p. 2601-9.
12. Ouwerkerk, R., et al., *Tissue sodium concentration in human brain tumors as measured with 23Na MR imaging.* Radiology, 2003. **227**(2): p. 529-37.

13. Ouwerkerk, R., et al., *Tissue sodium concentration in myocardial infarction in humans: a quantitative 23Na MR imaging study.* Radiology, 2008. **248**(1): p. 88-96.
14. Babsky, A.M., et al., *Predicting and monitoring response to chemotherapy by 1,3-bis(2-chloroethyl)-1-nitrosourea in subcutaneously implanted 9L glioma using the apparent diffusion coefficient of water and 23Na MRI.* Journal of Magnetic Resonance Imaging, 2006. **24**(1): p. 132-9.
15. Babsky, A.M., et al., *Monitoring chemotherapeutic response in RIF-1 tumors by single-quantum and triple-quantum-filtered (23)Na MRI, (1)H diffusion-weighted MRI and PET imaging.* Magn Reson Imaging, 2007. **25**(7): p. 1015-23.
16. Winter, P.M., et al., *Quantitation of intracellular [Na+] in vivo by using TmDOTP5- as an NMR shift reagent and extracellular marker.* J Appl Physiol, 1998. **85**(5): p. 1806-12.
17. Weber, L.W., M. Boll, and A. Stampfl, *Hepatotoxicity and mechanism of action of haloalkanes: carbon tetrachloride as a toxicological model.* Crit Rev Toxicol, 2003. **33**(2): p. 105-36.
18. Rao, P.S., R.S. Mangipudy, and H.M. Mehendale, *Tissue injury and repair as parallel and opposing responses to CCl4 hepatotoxicity: a novel dose-response.* Toxicology, 1997. **118**(2-3): p. 181-93.
19. Hernandez-Munoz, R., et al., *Balance between oxidative damage and proliferative potential in an experimental rat model of CCl4-induced cirrhosis: protective role of adenosine administration.* Hepatology, 1997. **26**(5): p. 1100-10.
20. Slater, T.F., *Free-radical mechanisms in tissue injury.* Biochem J, 1984. **222**(1): p. 1-15.
21. Nagano, K., et al., *Thirteen-week inhalation toxicity of carbon tetrachloride in rats and mice.* J Occup Health, 2007. **49**(4): p. 249-59.
22. Wu, X.L., et al., *Effect of Oxymatrine on the TGFbeta-Smad signaling pathway in rats with CCl4-induced hepatic fibrosis.* World J Gastroenterol, 2008. **14**(13): p. 2100-5.
23. Benyon, R.C. and M.J. Arthur, *Mechanisms of hepatic fibrosis.* J Pediatr Gastroenterol Nutr, 1998. **27**(1): p. 75-85.

24. Pierce, R.A., et al., *Increased procollagen mRNA levels in carbon tetrachloride-induced liver fibrosis in rats.* J Biol Chem, 1987. **262**(4): p. 1652-8.
25. Arthur, M.J., D.A. Mann, and J.P. Iredale, *Tissue inhibitors of metalloproteinases, hepatic stellate cells and liver fibrosis.* J Gastroenterol Hepatol, 1998. **13 Suppl**: p. S33-8.
26. Kawser, C.A., et al., *Rat hepatic stellate cell expression of alpha2-macroglobulin is a feature of cellular activation: implications for matrix remodelling in hepatic fibrosis.* Clin Sci (Lond), 1998. **95**(2): p. 179-86.
27. Winter, P.M., H. Poptani, and N. Bansal, *Effects of chemotherapy by 1,3-bis(2-chloroethyl)-1-nitrosourea on single-quantum- and triple-quantum-filtered 23Na and 31P nuclear magnetic resonance of the subcutaneously implanted 9L glioma.* Cancer Res, 2001. **61**(5): p. 2002-7.
28. Cameron, I.L., et al., *Intracellular concentration of sodium and other elements as related to mitogenesis and oncogenesis in vivo.* Cancer Res, 1980. **40**(5): p. 1493-500.
29. Koch, K.S. and H.L. Leffert, *Increased sodium ion influx is necessary to initiate rat hepatocyte proliferation.* Cell, 1979. **18**(1): p. 153-63.
30. Kline, R.P., et al., *Rapid in vivo monitoring of chemotherapeutic response using weighted sodium magnetic resonance imaging.* Clin Cancer Res, 2000. **6**(6): p. 2146-56.
31. Winter, P.M. and N. Bansal, *TmDOTP(5-) as a (23)Na shift reagent for the subcutaneously implanted 9L gliosarcoma in rats.* Magn Reson Med, 2001. **45**(3): p. 436-42.
32. Hubbard, P.S., *Nonexponential nuclear magnetic relaxation by quadropole interactions.* J Chem Physics, 1970(53): p. 985-987.
33. Colet, J.M., et al., *Multiple quantum filtered 23Na NMR spectroscopy of the isolated, perfused rat liver.* Magn Reson Med, 1999. **41**(6): p. 1127-35.
34. Steen, R.G., *Response of solid tumors to chemotherapy monitored by in vivo 31P nuclear magnetic resonance spectroscopy: a review.* Cancer Res, 1989. **49**(15): p. 4075-85.

35. Steen, R.G., et al., *In vivo 31P nuclear magnetic resonance spectroscopy of subcutaneous 9L gliosarcoma: effects of tumor growth and treatment with 1,3-bis(2-chloroethyl)-1-nitrosourea on tumor bioenergetics and histology.* Cancer Res, 1988. **48**(3): p. 676-81.
36. Kim, H., et al., *Induced hepatic fibrosis in rats: hepatic steatosis, macromolecule content, perfusion parameters, and their correlations--preliminary MR imaging in rats.* Radiology, 2008. **247**(3): p. 696-705.
37. Annet, L., et al., *Assessment of diffusion-weighted MR imaging in liver fibrosis.* J Magn Reson Imaging, 2007. **25**(1): p. 122-8.
38. Rockey, D.C. and D.M. Bissell, *Noninvasive measures of liver fibrosis.* Hepatology, 2006. **43**(2 Suppl 1): p. S113-20.
39. Desmyter, L., et al., *Rating of CCl(4)-induced rat liver fibrosis by blood serum glycomics.* J Gastroenterol Hepatol, 2007. **22**(7): p. 1148-54.
40. Kato, N., et al., *Effect of resovist on rats with different severities of liver cirrhosis.* Invest Radiol, 2002. **37**(5): p. 292-8.
41. Zuo, C.S., et al., *EVP-ABD-enhanced MRI to evaluate diffuse liver disease in a rat model.* Journal of Magnetic Resonance Imaging, 2008. **27**(6): p. 1317-21.
42. Brauer, M., R.A. Towner, and D.L. Foxall, *Sodium-23 and proton nuclear magnetic resonance imaging studies of carbon tetrachloride-induced liver damage in the rat.* Magn Reson Imaging, 1990. **8**(4): p. 459-65.
43. Towner, R.A., et al., *Use of 1H/23Na and 1H/31P double frequency tuned birdcage coils to study in vivo carbon tetrachloride-induced hepatotoxicity in rats.* Magn Reson Imaging, 1992. **10**(4): p. 679-88.
44. Brattin, W.J., E.A. Glende, Jr., and R.O. Recknagel, *Pathological mechanisms in carbon tetrachloride hepatotoxicity.* J Free Radic Biol Med, 1985. **1**(1): p. 27-38.
45. Lauria, V., et al., *[The physiopathological mechanism of hepatic fibrosis]*. Minerva Gastroenterol Dietol, 1998. **44**(3): p. 149-58.
46. Martinez-Hernandez, A. and P.S. Amenta, *The extracellular matrix in hepatic regeneration.* FASEB J, 1995. **9**(14): p. 1401-10.

CURRICULUM VITAE

Yong Gao

EDUCATION

2005 – 2008 Master of Science in Cellular and Integrative Physiology
Thesis: Noninvasive monitoring of CCl_4 induced acute and chronic liver damage in rat by single quantum and triple quantum filtered ^{23}Na magnetic resonance imaging
IUPUI, Indianapolis, Indiana

1995 – 1998 Master Degree in Clinical Pharmacology
Thesis: The Study of Pharmacokinetics of a Thrombin-like Enzyme from *Agkistrodon acutus* Snake Venom in Rabbits and Dogs
Medical University of Sun Yat-sen, Guangzhou, P.R. CHINA

1990 – 1995 Bachelor of Medicine Degree in Clinical Medicine
Henan Medical University, Zhengzhou, P.R. CHINA

PROFESSIONAL EXPERIENCE

Research Fellow in University of Tennessee at Memphis 2002 – 2005
Key Contributions:

- Using Tandem Affinity Purification method to purify the interacting protein partners of MSX3 fusion protein in lysate of C2C12 cells and 293 cells
- Protein identification with LCQ mass-spectroscopy

Research Associate in Guangzhou Medical College 1998 – 2001
Key Contributions:

- Purification of an anti-coagulant fraction in snake venom and toxicology study in mice
- Teaching pharmacology course for undergraduate students

LABORATORY SKILLS

- Collection and processing of ^{1}H and ^{23}Na MR Images, and ^{23}Na and ^{31}P MR spectra, with 9.4 Tesla Varian Magnetic Resonance System
- Cell culture of C2C12 cells, 293 cells, MDCK cells and RIF-1 cells

- Molecular biology techniques, including cloning, RT-PCR, protein expression, western, etc.
- Operation of LCQ mass-spectroscopy equipment
- Various surgeries on animals, including cannulation of coronary artery, femoral artery and vein in dogs, of jugular vein in mice and rats, and of bile duct in rats and rabbits

POSTERS AND CONFERENCES

- Y. Gao, J. R. James, N. Bansal. Monitoring Hepatic Cellular Damage by Single-Quantum and Triple- Quantum-Filtered Sodium MRI'. Oral presentation at RSNA 2008, 94th Scientific Assembly and Annual Meeting, Chicago, Illinois, November 30- December 5, 2008
- J. R. James, V. C. Soon, S. M. Topper, Y. Gao, N. Bansal. Non-invasive Controlled Radiofrequency Hyperthermia Using an MR Scanner and a Paramagnetic Thulium Complex. Poster presentation at 13th International Conference on Biomedical Engineering (ICBME2008), Singapore, December 3-6 2008
- J. R. James, Y. Gao, V. C. Soon, S. M. Topper, N. Bansal, Controlled Radiofrequency Hyperthermia & Simultaneous Monitoring of its Effects in Sc-implanted 9L-Glioma by *in vivo* ^{23}Na and ^{31}P Magnetic Resonance Spectroscopy. Poster presentation at 2008 World Conference on Interventional Oncology, Los Angeles, CA, June 22-25 2008

PUBLICATIONS

1. Gao Y, James JR, Bansal N. Monitoring rat liver injury in CCl_4 induced hepatotoxic model by SQ and TQF ^{23}Na MRI and ^{23}Na and ^{31}P MRS. (in preparation)
2. James JR, Gao Y, Soon VC, Topper SM, Babsky AM, Bansal N. Controlled RF HT Using an MR Scanner and its Simultaneous Effects on Sc-implanted 9L-glioma Tumors Monitored by ^{23}Na and ^{31}P MR Spectroscopy. (in preparation)
3. James JR, Gao Y, Miller MA, Babsky AM, Bansal N. Real Temperature Imaging with TmDOTMA. Magnetic Resonance in Medicine (under review)
4. Babsky AM, Topper S, Zhang H, Gao Y, James JR, Hekmatyar SK, Bansal N. Evaluation of extra- and intracellular apparent diffusion coefficient of sodium in rat skeletal muscle: effects of prolonged ischemia. Magn Reson Med. 2008 Mar;59(3):485-91

5. Tannu NS, Rao VK, Chaudhary RM, Giorgianni F, Saeed AE, Gao Y, Raghow R. Comparative proteomes of the proliferating C2C12 myoblasts and fully differentiated myotubes reveal the complexity of the skeletal muscle differentiation program. Mol Cell Proteomics. 2004 Nov; 3(11):1065-82. Epub 2004 Jul 30

6. Gao Yong, Long Qi-Cai. The Study of Pharmacokinetics of a Pure Fraction from Snake Venom with Thrombin-like Enzyme Activity in Rabbits. Academic Journal of Guangzhou Medical College, 1999;(2) 5-9